Use of Hadronic Calorimetry Information in the ATLAS Level-1 Muon Trigger

T. Ciodaro, J.M. de Seixas and A. Cerqueira on behalf of ATLAS Collaboration

***Abstract*—The ATLAS Tile hadronic calorimeter (TileCal) provides highly-segmented energy measurements for incident particles. Information from TileCal's last radial layer can assist in muon tagging and has been considered for inclusion in an upgraded Level-1 trigger. It can assist in the rejection of fake muon triggers arising from background radiation without degrading the efficiency of the trigger. This paper addresses the additional muon discrimination obtained by using a new receiver for the TileCal signals which interfaces with the current ATLAS Level-1 muon trigger. The design and performance of the receiver are also described.**

ATL-TILECAL-PROC-2013-006
19/06/2013

I. Introduction

THE ATLAS [1] particle detector operates at the Large Hadron Collider (LHC) at CERN. In order to measure the interesting final state properties of the collisions, ATLAS is divided into three subsystems (see Figure 1): the inner detector, responsible for tracking charged particles, the calorimeters, responsible for particle energy measurement and the muon system, responsible for muon identification and tracking. Furthermore, the inner detector and the muon system are immersed in solenoidal and toroidal magnetic fields, respectively, in order to produce bent trajectories for charged particles.

The ATLAS online trigger system is implemented in three cascaded levels, each possessing its own maximum event rate within the given latency [2]. The trigger system reduces the enormous data flow (60 TB/s) through the selection of events with interesting final state signatures. Due to processing speed requirements, the first level (Level-1, L1) is based on coarse information from the calorimeter and the muon systems. L1 is responsible for selecting regions of the detector in which significant information is available (RoI, Region of Interest). For this it uses energy and position information from the calorimeters and muon candidates from the muon system. The other two levels form the so called high-level trigger (HLT), which has access to the full granularity and resolution of the detector within the RoI, and is able to confirm or reject the L1 decision [3].

In particular, this work addresses the L1 trigger for muons in the ATLAS central barrel region. The L1 trigger uses information from Resistive Plate Chambers (RPC) in the muon system to identify muon candidates [4]. Two main sources of fake triggers degrade the L1 performance for muons, especially at high luminosities. The first arises from beam-associated photon and neutron fluxes in the ATLAS cavern [5], while the second is associated with muons from in-flight decays of pions and kaons. Combining calorimetry and RPC information to reduce the fake rate was conceived in the original ATLAS design, but its implementation was left for a future upgrade [6].

T. Ciodaro is with the Signal Processing Laboratory - COPPE/Poli, Federal University of Rio de Janeiro, Brazil (e-mail: ciodaro@cern.ch).

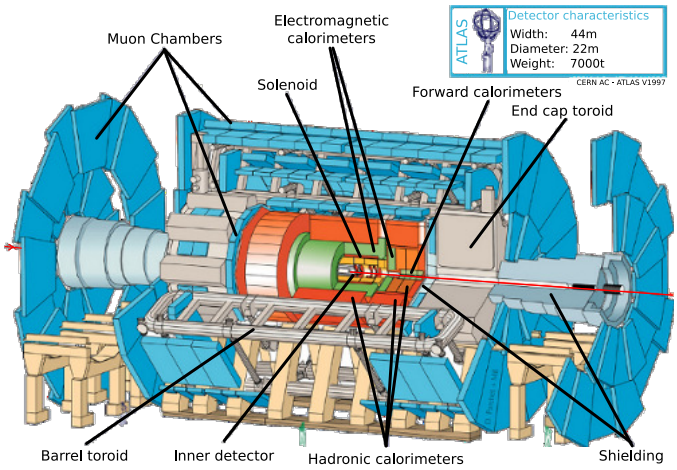

Figure 1. The ATLAS detector.

This paper presents a study of the use of information from the ATLAS barrel hadronic calorimeter (TileCal) to assist in muon tagging. This could be implemented as part of an L1 upgrade. Signals from TileCal are transmitted to a muon receiver, which interfaces with the ATLAS L1 muon trigger. As the muon interaction in the calorimeter produces small signals, the muon receiver adds the two signals from the same calorimeter cell to improve the signal-to-noise ratio. For signal detection, the summed signal is presented to a matched-filter-based digital discriminator. Data from experimental tests with muon beams are used in circuit simulations to evaluate the receiver design performance. The L1 muon performance is evaluated using proton-proton collision data, through the combination of both TileCal and RPC information.

The paper is organized as it follows. Section II and Section III describes the Tile Calorimeter and Muon Systems respectively. Section IV is dedicated to the muon receiver and Section V describes the signal-to-noise improvement in the muon receiver scheme. Signal discrimination against noise is discussed at Section VI, together with the matched-filter-based discriminators. Section VII presents the results from the combined muon trigger, while conclusions are reported in Section VIII.

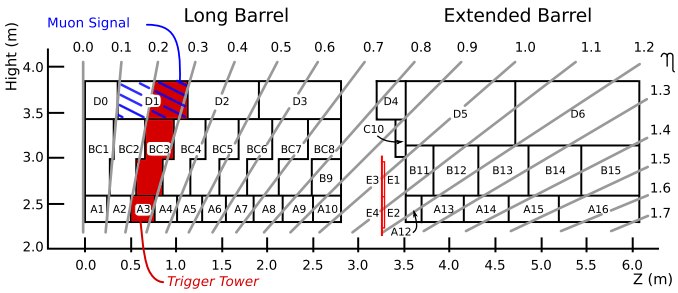

Figure 2. The TileCal cell geometry, consisting of 3 radial layers and a pseudo-projective layout.

II. The Tile Calorimeter

The TileCal detector [7] is a hollow cylinder consisting of 64 modules arranged in φ[1]. It is a sampling calorimeter [8] with steel plates as the primary absorber and plastic scintillator tiles as the active material. The tiles in each module are grouped together into readout cells (see Figure 2). Charged particles produce scintillation light in the plastic tiles and wave-length shifting fibers collect the scintillation light and transport it to photomultiplier tubes (PMT). The PMTs convert the light into electrical signals, whose amplitude, after pulse shaping, is proportional to the deposited energy. Then, the electrical signals are digitized and read out by the back-end electronics if the event is accepted by L1 [9]. Two sides of each calorimeter cell are connected to independent PMT's and thus two independent readout channels, providing redundancy to the data acquisition (left and right channels).

The TileCal L1 interface card processes two analogue signals [10]. The first is a trigger tower signal (the sum of all cell signals in the shaded region in Figure 2), spanning 0.1×0.1 on the $\eta \times \varphi$ plane. It is used by the calorimeter trigger. The second is the muon signal, which is formed by amplifying the signal from the outermost calorimeter layer (D cells). Each D cell provides two muon signals: one from the left readout (DL), and one from the right readout (DR).

In total, TileCal provides approximately 10k readout channels. For the L1 trigger, ≈3.5k tower and muon signals are transmitted. TileCal is also divided into two regions according to the beam axis (z), which allows infrastructure and services to reach the inner most detectors: the long and extended barrels. Together with the entire ATLAS detector, the calorimeter is logically split into A and C sides, according to the η sign. Note that the cell in $\eta = 0.0$ (D0) is split into the A and C sides: one signal is read out by the A side electronics, while the other is read out by the C side.

Currently, the TileCal muon signals are available at the L1 calorimeter patch panel, in the ATLAS electronics cavern. Later, these muon signals may be connected to the muon receiver described in this article.

[1]The azimuthal angle ϕ is measured around the beam axis. The pseudorapidity η is defined as $\eta = -\ln\left(\tan\frac{\theta}{2}\right)$, where θ is the polar angle measured from the beam axis (z).

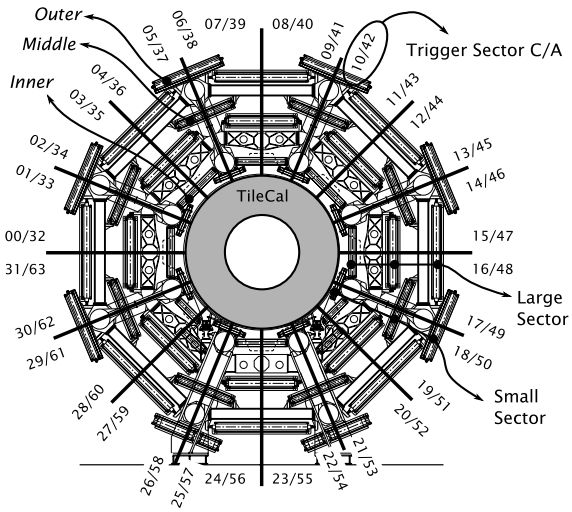

Figure 3. Muon system layout.

III. Muon System

The ATLAS muon system identifies and tracks particles within a toroidal magnetic field. In the barrel region, RPC detectors are used to tag muons for the L1 trigger, while MDT stations are used for fine tracking in the HLT [11]. Physically, the muon system is divided in the φ-coordinate into 8 Large and 8 Small Sectors, both equipped with several MDT and RPC chamber assemblies. The muon system geometry can be seen in Figure 3.

In the trigger logic, the muon system is divided into 64 trigger sectors, in the φ-coordinate, 32 per detector side (A and C), representing a granularity of 1.05×0.2 in the $\eta \times \varphi$ plane. The first 32 sectors are on the C side (from 0 to 31) while the last 32 sectors (from 32 to 63) are on the A side. Each trigger sector is capable of producing multiple RoIs. Physically, RPC's are positioned in three distinct planes [4]. Muons hit the three planes and are classified within 6 p_T thresholds. The information from a trigger sector is fully received by a Sector Logic (SL) board, which also has the infrastructure to receive TileCal information (through the MUCTPI interface boards) [4]. These boards interface the SL with the MUCTPI, which interfaces the entire muon system with the Central Trigger Processor (CTP) [2]. Due to mechanical layout choices, trigger sectors overlap, leading to a double counting of muons, which is handled by the MUCTPI.

MDT information within the RoI previously selected by L1 is used to confirm the RPC muon candidate at the HLT. The reconstructed muon track provides a better resolution for the muon p_T. MDT information is also used by offline algorithms to extrapolate the muon track to the calorimeters and inner detectors [12].

IV. Muon receiver

A prototype receiver for the TileCal muon signals has been developed to extract information from the signals and to discriminate them from noise [13]. Figure 4 shows the organization of the system and its interface with the RPC off-detector electronics. Analogue muon signals from TileCal

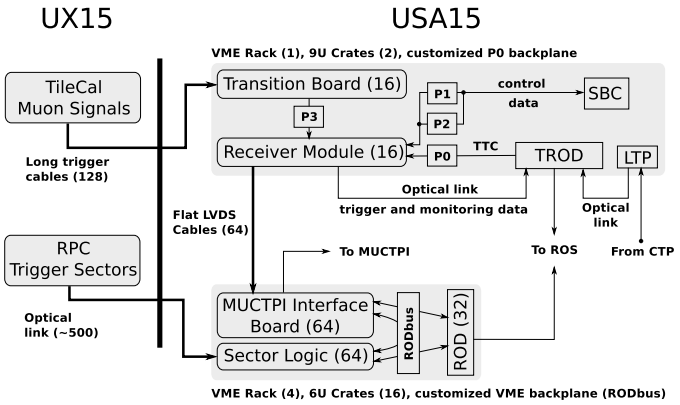

Figure 4. Organization and interfacing of the TileCal muon signals with the muon trigger system.

are transmitted from the experimental cavern (UX15) to the electronics area (USA15), where the radiation from particle collisions is substantially reduced. The signals enter transition boards at the back of VME crates where they are remapped and transmitted to receiver modules at the front of the crate.

The information extracted by the receiver boards, such as the cell energy and bunch-crossing number, is sent to both the Sector Logic (SL) boards for interfacing with the RPC triggers, and to the Trigger Readout Driver (TROD). The TROD codes and packs the receiver module data and interfaces it with the ATLAS readout system (ROS). The TROD also receives trigger information from the Local Trigger Processor (LTP) and distributes it to the receiver modules through a dedicated *P0* space on the VME bus. Other modules needed in the VME crate include the Single Board Computer (SBC) crate controller which communicates with the modules through an Ethernet connection.

A. Coverage

Figure 5 shows the distribution in the $\eta \times \varphi$ plane of simulated single muons crossing the muon spectrometer in regions not instrumented with RPC's (areas with black dots). The central gap around $|\eta| \approx 0.0$ is associated with infrastructure services where cables and pipes run to various detector systems. The uncovered regions in $-2.3 < \varphi < -1.7$ and $-1.4 < \varphi < -0.9$ correspond to the magnet support structures. Other patterns can also be seen in Figure 5, and the total uncovered area corresponds to $\sim$20%.

The muon trigger system could profit from overlapping the instrumented regions of both the TileCal and RPC systems, with TileCal tagging muons crossing some of the uninstrumented RPC regions. The region corresponding to the magnet support structure corresponds to more than one D cell and its implementation is more complex. The RPC central gap can be recovered by the TileCal D0 cell, but would have to trigger muons independently from RPC trigger. Although possible, it is unfeasible today because the muon momentum cannot be estimated from TileCal energy measurements, as needed for the present HLT architecture.

Further, in order to reduce the complexity, the TileCal extended barrels are not considered in the receiver's design. Projective muons with $|\eta| > 1.05$ traverse the extended barrel modules and generally the thin-gap trigger chambers (TGCs) in the muon end-caps rather than the RPC detectors in the barrel region.

B. Muon matching

To trigger correctly on muon signals from both the TileCal and RPC detectors, their geometries and the bunch-crossing identification (BCID) must be matched. The BCID indicates the LHC bunch crossing associated with the signal.

The BCID is deduced from the peak of the TileCal muon signal. As the time elapsed between the muon crossing the calorimeter and the measured peak time is fixed, knowing when the signal peak occurs leads to the BCID. Circuit calibration is needed to exactly estimate the signal peak time. The BCID for the TileCal signal is sent to the SL boards for matching with the BCID for the RPC signal.

The geometrical matching is performed through the RPC trigger sectors. Each TileCal D cell is mapped onto one trigger sector (see Figure 3). When a D Cell signal satisfies the receiver module, its trigger sector is sent to the corresponding SL board. If an RPC RoI is triggered in that same trigger sector, it is presumed that both TileCal and RPC were triggered by the same muon and thus L1 is triggered. Muons triggering the TileCel D cell at $|\eta| \approx 0.0$ (see D0 cell in Figure 2) flag two trigger sectors because this cell has the standard length of $\Delta\eta = 0.2$ but spans the A and C sides of the detector. As a trigger sector is handled by one SL board, the matching is also referred to as SL matching.

As already mentioned, only the TileCal long barrel signals are processed by the receiver. Thus, an RPC RoI with $|\eta| > 0.7$ will trigger L1 without TileCal confirmation.

V. Signal-to-Noise Ratio Improvement

The characteristics and detection capability of the TileCal muon signals have been thoroughly investigated in experimental beam tests [15]. It has been shown that the summing both muon signals from the same D cell increases the signal-to-noise ratio (SNR) by a factor of $\sim\sqrt{2}$ (assuming uncorrelated

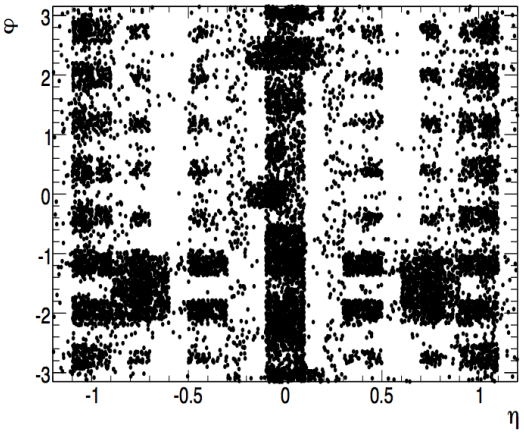

Figure 5. The RPC uncovered regions [14]. The black dots correspond to reduced acceptance.

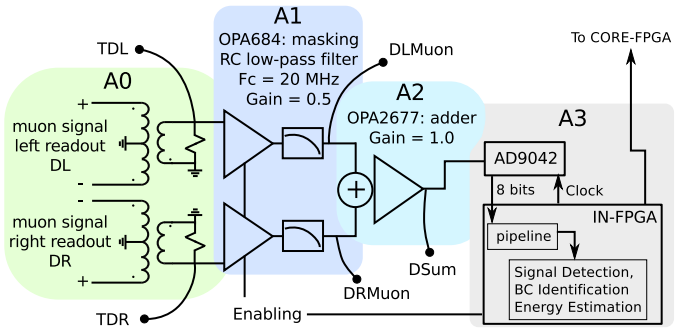

Figure 6. Basic design for signal receiving in the receiver module.

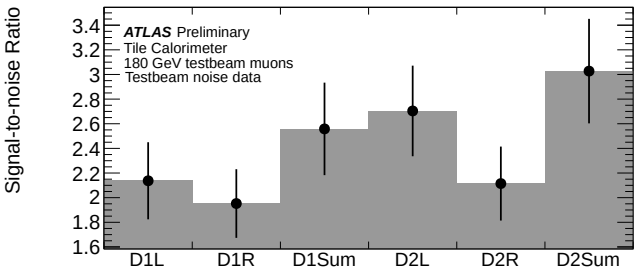

Figure 7. Signal-to-noise ratio for signals from the D1 and D2 cells of the Tile Calorimeter, together with the output from the summing circuit. These results are derived from circuit simulations using measurements with 180 GeV muon beams [17].

noise). The same approach is followed in the muon receiver by analogue summing of the muon signals from the same D cell.

Figure 6 shows the basic design for signal receiving in the receiver module. After converting the TileCal differential signals to single ended (A0) and buffering them (A1), a low-pass RC filter limits the signal bandwidth to 20 MHz. Note that the buffer amplifiers (A1) can be disabled in order to mask noisy channels. The resulting analog signals are summed (A2) before being digitized by the AD9042 [2] at 40 Msps with 8-bit resolution (the 4 LSB are not significant). The digital samples are transferred to an FPGA which performs signal discrimination, energy estimation, and BCID determination.

A. Circuit performance

The summing circuit was evaluated with PSpice [16] simulations using TileCal muon signals recorded during experimental beam tests. Projective muon beams of fixed energy hit TileCal at a series of different η values. For these tests, a special setup was used to acquire the muon signal from each PMT with a 40 Msps, 8-bit resolution FADC [15]. The noise properties of the signals were obtained from data taken without the presence of beam (pedestal runs). Here, the data analysis is performed for two D cells (D1 and D2 in Figure 2), from one TileCal module used during the tests.

The digitized samples were converted back to voltage and used as inputs to the PSpice simulation, for both the muon and noise signals. After summation of the two PMT signals, the pulse was digitized again, simulating the AD9042, and 5 samples around the expected peak sample, were stored. The IN-FPGA is able to adjust the digitalization clock to match the peak sample, within 1 ns resolution, which is needed for BCID. Also simulations of the frequency response and noise contribution of the summing circuit were performed.

The summing circuit uses RC low-pass filters (A1 in Figure 6) and simulations showed a cut-off frequency (3 dB) of 19.50 MHz, suitable for the FADC sampling rate. The muon signal bandwidth is 8 MHz and is not significantly affected by the cut-off frequency. From Figure 6, the circuit gain is 0.5, when the output is compared to a single input (DL or DR). This avoids signal saturation at the output node (DSum).

[2]A 12-bits, 41 MSPS monolithic analog-to-digital converter from Analog Devices.

The simulation predicts that the circuit contributes an RMS noise of $\sim$46 μV, which is negligible compared to the total input noise from the TileCal electronics of $\sim$18 mV.

The signal amplitude, which is proportional to the energy deposited by the muon, must be estimated from a fit to the expected muon signal pulse shape (from circuit simulation), for the digitized signals at DL, DR, and DSum. The circuit linearity is then measured with the total energy represented by the muon signals before (DL and DR) and after signal summation (DSum). The DSum nonlinearity, measured by the maximum deviation from the linear model, was estimated as $\sim$0.92% for D1, and $\sim$0.83% for D2.

The SNR before and after the summing circuit was also evaluated for both D1 and D2 cells. The SNR is defined as the ratio between the most probable value (MOP) of the estimated energy distribution for the muon signals, and the RMS of the noise distribution [15]. Figure 7 shows the SNR at different circuit nodes (D1L, D1R and D1Sum, as the left, right, and summing readout of the D1 cell, and similarly for the D2 cell). Considering the input SNR as the average value between the SNR at DL and DR, the SNR gain between the input and output is $\sim$1.25$\pm$0.26 for D1, and $\sim$1.26$\pm$0.25 for D2, both consistent with the expected $\sqrt{2}$. The increase in SNR of D2Sum relative to D1sum is due to the larger path length through the calorimeter at higher η and hence a larger signal. For the sake of comparison, the SNR of the summed muon signals from the extended barrel is greater than 5.0 because of the thicker cells and greater η. This leads to almost $\sim$100% signal detection with a negligible misidentification rate [15]. The SNR achieved by the summed muon signal in the barrel is not sufficient for perfect signal discrimination.

VI. Signal discrimination

The IN-FPGA of the receiver module (see Figure 6) receives the digitized samples from the AD9042. Signal discrimination and BCID determination use 5 digitized samples, and are performed each time a new sample is read. It is well-known in signal detection theory that a matched filter is the optimal linear discriminator based on SNR [18]. This discriminator bases its decision on a hypothesis test applied to the received signal (see Equation 1). For hypothesis H_0 there is no signal ($s[i]$) and only noise ($n[i]$) is received. For hypothesis H_1

the signal of interest is present, but is corrupted by additive noise.

$$\begin{aligned} H_0 : r[i] &= \quad n[i] \\ H_1 : r[i] &= \quad n[i] + s[i], \quad i = 1, 2, ..., 5 \end{aligned} \tag{1}$$

The likelihood ratio is defined as the ratio of the joint probability density functions ($pdfs$) of the received signals interpreted by the two hypotheses, and is the best measure of how likely a received signal is from H_1 or H_0. The definition is

$$\Lambda(\mathbf{r}) \triangleq \frac{p_{\mathbf{r}|H_1}(\mathbf{r})}{p_{\mathbf{r}|H_0}(\mathbf{r})} \underset{H_0}{\overset{H_1}{\gtrless}} \gamma \tag{2}$$

where $p_{\mathbf{r}|H_n}(\mathbf{r})$ is the pdf of the received signal $\mathbf{r}$ under hypothesis H_n (where $n = 0$ or 1). Therefore, a decision favoring H_1 is taken whenever $\Lambda(\mathbf{r})$ is greater than a detection threshold value (γ).

Two versions of the matched filter discriminator are discussed here. A simplified approach considers the muon signal to be represented by the mean value over all the events of the muon signal, calculated for each calorimeter cell. Despite muon signal stochasticity, this simplification aims at reducing the discriminator complexity, which is quite attractive for online implementation. A full stochastic matched filter design considers, also for simplicity, both muon and noise signals to be Gaussian random processes.

A. Simplified Approach

Assuming that the received noise is white, zero-mean Gaussian ($n[i]$), the likelihood ratio in Equation 2 can be simplified to

$$\Lambda(\mathbf{r}) = \sum_{i=1}^{5} r[i]m[i] \tag{3}$$

where $m[i]$ is the i-th sample of the mean signal from the muon signals in the development set.

Therefore, one has to correlate the mean muon signal with the received signal and classify this received signal as muon or as noise depending on a given discrimination threshold.

B. Stochastic Approach

The full stochastic design can be simplified when the signal of interest is Gaussian [19]. Uncorrelated Gaussian signals are also independent. Thus, the joint pdf in Equation 2 can be factorized into a product of Gaussian distributions.

For Gaussian signals, the Karhunen-Loève representation is applied, resulting in a finite set of constants (λ_k) and orthonormal vectors ($\varphi_k[n]$), which are, respectively, the eigenvalues and eigenvectors of the autocorrelation matrix of the given stochastic process [20]. A signal from the stochastic process ($r[i]$) can be mapped onto this representation without loss of information:

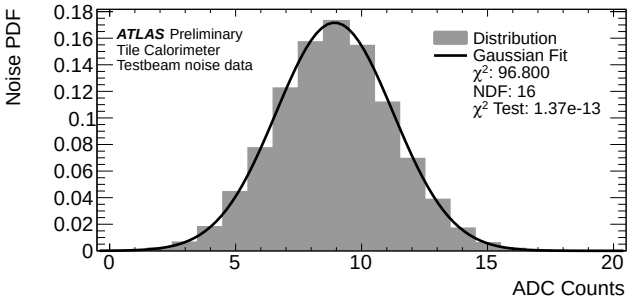

Figure 8. Gaussian fit for digitized noise samples from the D1 cell, as derived from circuit simulations based on measurements with 180 GeV muon beams [17].

$$\begin{aligned} r_k &= \sum_{i=1}^{5} r[i]\varphi_k[i] \\ r[i] &= \sum_{k=1}^{5} r_k\varphi_k[i] \end{aligned} \tag{4}$$

where the coefficients r_k are uncorrelated and, as they are Gaussian, independent. In this way, the received signals are mapped onto the eigenvectors $\varphi_k[i]$ and the likelihood ratio in Equation 2, after some simplifications, can be computed as [19]:

$$\begin{aligned} \Lambda(\mathbf{r}) = \frac{1}{N_0}\Bigg(&\sum_{i=1}^{5}\sum_{j=1}^{5} r[i]r[j]\left[\sum_{k=1}^{5}\lambda_k d_k\right] \\ &+ \sum_{i=1}^{5}\sum_{j=1}^{5} m[i]r[j]\left[\sum_{k=1}^{5} d_k\right]\Bigg) \end{aligned} \tag{5}$$

where $d_k = (\lambda_k + N_0/2)^{-1}\varphi_k[i]\varphi_k[j]$. Again, $m[i]$ is the signal corresponding to the mean energy deposited by muons. Also, this approach requires the received noise to be white: the noise spectral density is constant over all frequencies, with value $N_0/2$, which can be estimated from the noise covariance.

C. Implementation

The PSpice simulated signals (see Section V-A) were used to evaluate the performance of the proposed discriminators. Both the noise and muon signal data sets were split into two large subsets of similar size: the development set used for discriminator design, and the test set used for performance evaluation. A separate discriminator was developed for each D cell (D1 and D2 for this test beam case).

The matched-filter discriminators were developed assuming that the TileCal noise is Gaussian. This hypothesis was submitted to a χ^2 test, which is a natural choice for evaluating data models. Figure 8 shows the noise samples distribution and the respective Gaussian fit. This result accumulates noise samples from the D1 cell.

Despite the reasonable Gaussian behavior, the χ^2 test rejected the Gaussian model. The χ^2 test is very sensitive and, thus, the Kullback-Leibler divergence [21], as a measure

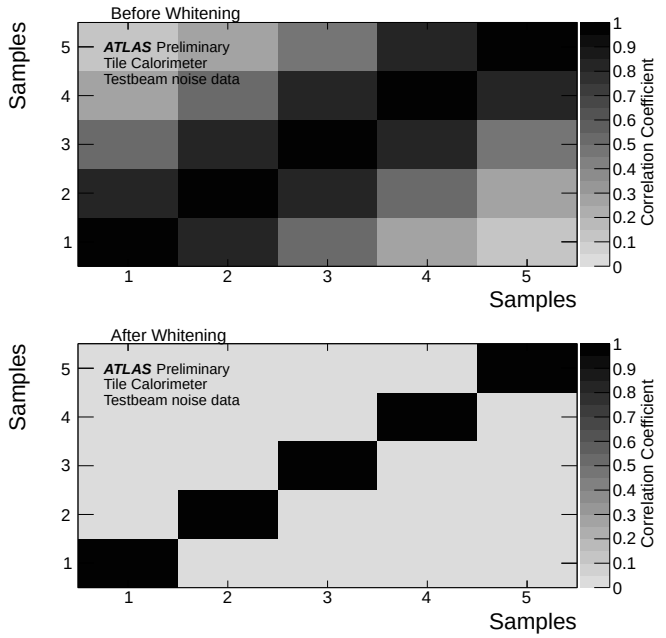

Figure 9. Covariance matrices from the test set before and after whitening, for noise signals from the D1 cell. These results are derived from circuit simulations based on measurements with 180 GeV muon beams [17].

of similarity between two distributions, was employed. The Jensen-Shannon test [21] goes between zero, for completely different distributions, and one, for similar ones. In order to compare to the Gaussian model, a distribution with the same number of noise observations was obtained from a random Gaussian generator, keeping the same mean and variance as for the noise sample distribution. The test returned 0.9997, for the D1 cell, and 0.9999 for the D2 cell, indicating that the noise sample distributions are not far from a Gaussian model.

Also, the TileCal noise is not white, thus, a whitening stage [19] must be implemented before applying the matched filter. Noise samples from the development set are used to implement the whitening stage [22], through the computation of the eigenvalues and eigenvectors of the noise covariance matrix for the 5 digitized samples.

Figure 9 shows the covariance matrix of the test set before and after whitening. It can be seen that consecutive noise samples are correlated before the whitening stage. After, the 5 noise pulse digitized samples are completely uncorrelated and, assuming Gaussian hypothesis, statistically independent. Finally, it can be seen that the whitening stage designed from the development set satisfactorily generalizes the result for the test set.

In order to correctly apply the matched filter approaches described earlier, both muon and noise signals must be applied to the whitening stage. After, the mean muon signal, together with the eigenvectors and eigenvalues (for the stochastic approach) of the autocorrelation matrix, are derived from the muon signals of the development set.

Several studies concerning the TileCal response for muons showed that the muon energy deposited in a cell follows a Landau convolved with a Gaussian distribution [15]. As the discrete time muon signal has an intrinsic dependence on

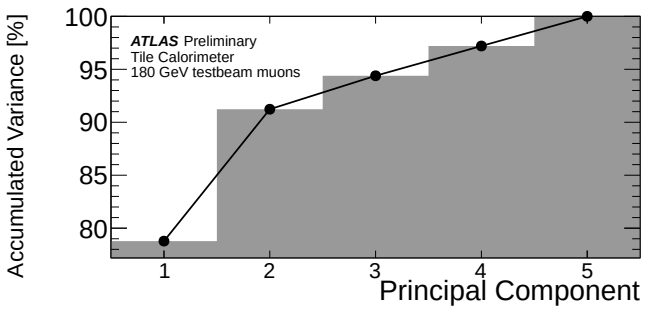

Figure 10. Charge curve for Principal Component extraction from summed muon signals for muons crossing the D1 cell. These results are derived from circuit simulations based on measurements with 180 GeV muon beams [17].

the deposited energy, signal samples whose distributions are considerably different from noise should follow a distribution similar to the energy distribution. Nevertheless, the Gaussian approach (which is not far from the actual muon deposited energy distribution for low signals [15]) was implemented.

The Karhunen-Loève representation of digital signals can be obtained using principal component analysis (PCA) [20]. The design of the discriminator using the stochastic approach requires the PCA to be performed over the muon signals without the presence of noise. This is unrealistic in many applications, and the PCA was evaluated from received signals under the H_1 hypothesis. Furthermore, PCA can also be used to compact the information by ranking the principal components (PC) according to their variance and excluding components with insignificant variance [20], which is attractive for L1 operation where speed is important. Instead of using all the PCs, just those which represent a given fraction of the total data variance are used, reducing the total number of operations needed for signal discrimination.

Figure 10 shows the charge curve for the PCA extracted from the summed muon signals from the D1 cell (sum of D1L and D1R signals) using the only the development set. It can be seen that the two first PC have more than 90% of the total data variance. Signals from the D2 cell show a similar behavior.

D. Results

The discrimination performance is evaluated from the test set through the ROC (Receiver Operating Characteristics) curve [18], which shows the behavior of the muon signal detection efficiency with respect to the false alarm rate, as the discrimination threshold γ is lowered. Figure 11 shows the ROC curves for the discriminators applied to the summed muon signal for both the D1 and D2 cells. Performance is shown for the simplified matched filter, the stochastic matched filter considering all principal components, the first component only, and the first two components only.

Table I summarizes the signal detection efficiency for a fixed false alarm of 10%. Besides the matched-filter-based discriminators, the performance of a threshold discriminator over the digitized samples can also be considered for completeness. Its performance is much below the matched filter discriminators shown in Figure 11. The performance of the

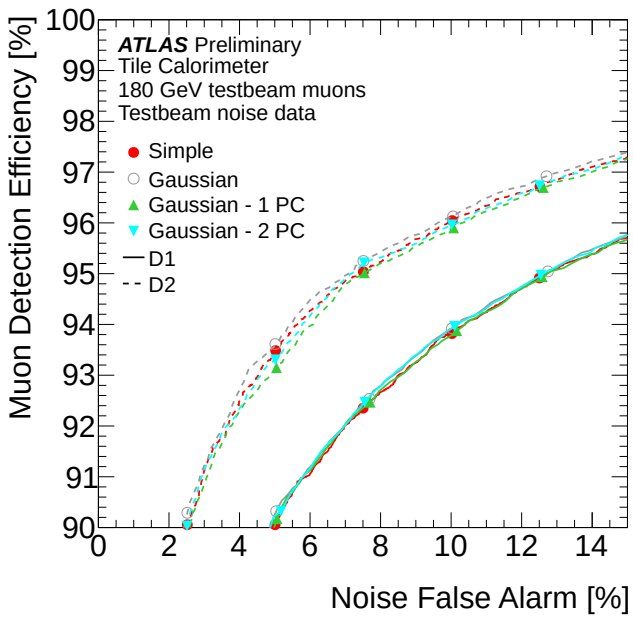

Figure 11. ROC curves for designed matched filters for TileCal cells D1 and D2. A ROC curve for a simple threshold discriminator over the digitized samples is much lower and cannot be seen. These results are derived from circuit simulations using signals from measurements with 180 GeV muon beams [17].

four matched filter discriminators are comparable. Although the stochastic approach achieves a performance slightly better than the simplified approach, the latter is considered the most appropriate for the muon receiver, due to its simplicity and speed.

The energy deposited in the D cell by the muon can be estimated from the output of the simplified matched filter approach, as can be seen in Figure 12. The fitted linear model can be used to convert from the simplified matched filter output to energy. Only summing signals whose discriminator output is greater than three times the respective RMS noise level (noise signals processed by the simplified matched filter discriminator) are considered for the linear model. This is important when trying to estimate the energy cut that is being applied to D cells through the simplified matched filter. As the muon energy deposition depends on η and the fitted linear model depends on the noise level, each cell should have its own calibration factor. For Table I, the corresponding threshold was set to $\sim$280 MeV.

VII. Combined Trigger Performance

Although the main purpose of combining the TileCal and RPC information is to reduce the fake trigger rate, the combination should also not degrade the L1 muon performance. While no accurate simulation is available to predict the fake RPC trigger rate from radiation effects, the impact of the combined trigger scenario on the present L1 performance has been addressed by using proton-proton collision data together with a Monte Carlo simulation.

Muon signals from eight TileCal long barrel modules were analyzed, covering approximately the region $|\eta| < 0.7$ and

Table I
Detection efficiency for a fixed false alarm of 10%.

Cell	Discriminator Efficiency (%)				
	Matched Filter				Threshold γ
	Simplified	Gaussian			
		All PC	1 PC	2 PC	
D1	93.8	93.8	93.8	93.9	87.7
D2	96.0	96.1	95.9	95.9	91.7

$-0.9 < \varphi < -0.5$ (referred to here as the *data region*). This region is approximately centered and well contained within one of the Large Sectors of the muon system shown in Figure 3. The region corresponds to two trigger sectors in φ.

Using offline tracking, the full muon trajectory can be determined, from the interaction point through the calorimeter and muon systems, taking into account the effect of the magnetic field. The muon detected offline can be matched to the L1 RoI selected by the RPC system by requiring $\Delta R \equiv \sqrt{\Delta\eta^2 + \Delta\varphi^2} < 0.5$ between the track position at the muon system and the RoI coordinate. The TileCal D cell crossed by the track can also be determined. This allows the trigger sectors of the RoI and TileCal D cell to be assigned. Using this information, the impact of requiring the D cell in the trigger can be evaluated both for data and Monte Carlo events.

A. Sector Logic Mismatches

Monte Carlo simulations of single muons with a wide variety of transverse momentum were studied. The SL matching described in Section IV-B requires that a muon be assigned to the same trigger sector in both the TileCal and the RPC. An SL mismatch occurs when they are assigned to different sectors. This can occur because of incomplete geometrical overlap of the two trigger sectors, muon scattering in the material, or muon trajectory deviation by the magnetic fields. For these reasons, low-p_T muons tend to fail the SL matching more frequently than high-p_T muons.

The SL mismatch can be handled by the MUCTPI with a simple addition to the logic. If the trigger sector assigned to the muon by RPC and the one assigned by the TileCal muon receiver are contiguous, it can be assumed that the mismatch was due to the reasons previously described and the muon accepted. If the muon trajectory deviation is greater

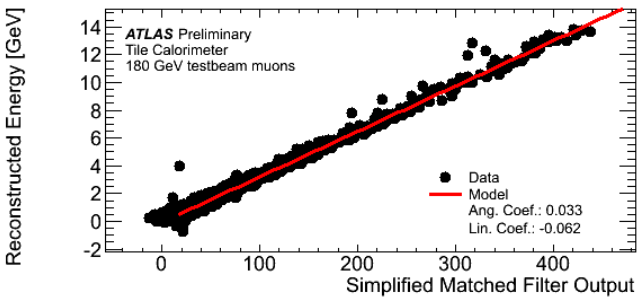

Figure 12. D cell energy estimation through the simplified matched filter output (Equation 3). These results are derived from circuit simulations using measurements with 180 GeV muon beams [17].

than two trigger sectors ($|\varphi| > 0.4$), it still fails the SL matching. When this adjustment is made for the Monte Carlo events, the SL mismatch is negligible. Also, as most of the interesting physics channels involve high-p_T muons, the impact of the mismatch on physics analysis would be even smaller. Eventually, this compensation would also affect the cavern background rejection.

B. Collision data

Spare hardware from the ATLAS L1 system was used to record some of the TileCal muon signals during proton-proton collisions in ATLAS. These muon signals were connected to the same hardware used to read the trigger tower signals and were hence available for offline analysis. In total, 56 muon signals from 28 D cells of the long barrel region were recorded for each event (*data region*). As in the muon receiver, the signals were digitized at a 40 Msps rate. Reprocessed single muon data from 2010 (periods H and I) were used to study the combined trigger performance. The events in the collision data sample were triggered by the muon system and were selected if they passed the pre-defined transverse momentum thresholds for L1. Further selections were applied offline, requiring at least one reconstructed muon track fulfilling the tight identification criteria [23] with offline p_{T} greater than 25 GeV if it was isolated; otherwise greater than 75 GeV. In the presence of two reconstructed muons the p_{T} threshold was set at 15 GeV. Muons with smaller p_{T} were also selected if other particles, such as electrons and jets (with their p_{T} criteria) were present in the event. For the final study, only muons crossing the 28 D cells of TileCal and triggering by the RPC were considered. A given event is considered for the noise analysis if there are no muons crossing the calorimeter in the long barrel region (as the proposed muon receiver uses only information from long barrel D cells).

As was done for the Monte Carlo studies, the tracking of offline reconstructed muons was used for the muon detection analysis. The compensation described in Section VII-A was applied to reduce the inefficiency due to SL mismatches. Instead of simulating the summing circuit in PSpice, the digital samples of the muon signals from the same D cell were summed by software. The simplified matched filter discriminator previously discussed was implemented following the methodology described in Section VI-C. For estimating the cell energy through the output of the simplified matched filter, signals from all 28 cells were used in order to increase statistics.

Figure 13 shows the probability that a muon triggered by RPC is confirmed by the TileCal muon receiver, as a function of the applied discriminator threshold (converted to energy). It can be seen that a threshold of $\sim$350 MeV, would give a muon detection efficiency of $\sim$80%. Also, it is shown the probability that the TileCal muon receiver confirms a SL in the absence of muons in the long barrel, in a hypothetical scenario where RPC triggered a ROI from a fake muon. For that same energy threshold, the TileCal muon receiver would confirm 20% of the SL misidentified by RPC, because of the TileCal D cell noise.

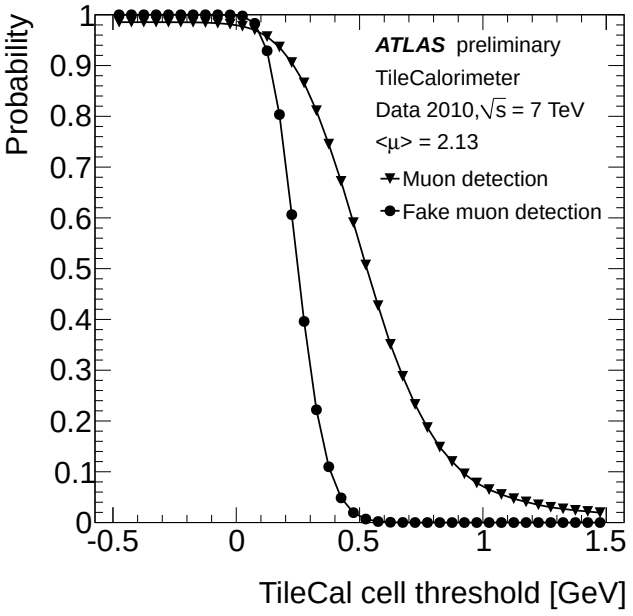

Figure 13. Probability that the receiver system confirms the muon triggered by RPC, with respect to the energy threshold based on the TileCal rear sampling information available at L1. It is also shown the probability that the receiver system would confirm a RPC sector logic in the absence of muons crossing the long barrel, given the hypothetical scenario where RPC has already misidentified a muon [17].

VIII. Conclusions

A combined muon trigger using both TileCal and RPC information for the ATLAS L1 trigger has been studied. A muon receiver for the TileCal muon signals was developed and issues concerning the muon signal discrimination from noise were investigated through the development of matched-filter-based discriminators, using data from experimental beam tests. The simplified matched filter design showed the best compromise between performance and simplicity and was the baseline used for testing the system performance with proton-proton collision.

The results from Monte Carlo simulations and proton-proton collision data showed good agreement with respect to Sector Logic mismatch. Because of implementation constraints, only signals from a specific region of the detector could be analyzed. The discriminator designed in this study was able to detect muons while keeping the probability of confirming fake muons low.

A. Discussion

The TileCal signal from the last calorimeter layer has been proposed to reduce the fake muon rates in the L1 trigger. Several experimental studies with muon beams were performed to evaluate its discrimination capability [15]. The integration between the TileCal signals and the RPC trigger, however, was left for a future upgrade in case the fake muon rate increased beyond the design safety factor.

Recent background estimates for high luminosity scenarios and 14 TeV collisions show that the fake rates due to the cavern radiation are below the design safety factors. Also,

muons from inflight decays of pions and kaons, which are a second source of fake muons in the L1 trigger, are not as dangerous as initially expected. Thus, based on present knowledge, it was concluded that a combined L1 trigger involving both TileCal and RPC is not mandatory and can be left as a backup in case the L1 fake rates do not behave as currently predicted.

However, depending on the trigger strategy for the earlier phases of the upgrade, the TileCal muon signal might be considered. Some thoughts and discussions to use it as a trigger for the muon MDT chambers have brought back attention to this matter.

ACKNOWLEDGMENT

We are thankful for the support that has been provided to this study by CNPq, CAPES, FINEP, RENAFAE, FAPERJ and FAPEMIG (Brazil), CERN and the Europe Union (through the HELEN program). We would also like to thank our colleagues from both ATLAS TileCal and TDAQ collaborations for all the support and interesting discussions concerning this work.

REFERENCES

[1] The ATLAS Collaboration, "The ATLAS experiment at the CERN large hadron collider," *Journal of Instrumentation*, vol. 3, no. S08003, 2008.
[2] K. Kordas et al., "The ATLAS data acquisition and Trigger: concept, design and status," *Nuclear Physics B - Proceedings Supplements*, vol. 172, pp. 178 – 182, 2007.
[3] S. Wheeler et al., "An Overview of the ATLAS High Level Trigger Dataflow and Supervision," *IEEE Transactions on Nuclear Science*, vol. 51, pp. 361–366, 2004.
[4] F. Anulli, G. Ciapetti, et al., "The Level-1 Trigger Muon Barrel System of the ATLAS experiment at CERN," *Journal of Instrumentation*, vol. 4, no. 04, p. P04010, 2009.
[5] S. Baranov, M. Bosman et al., "Estimation of radiation background, impact on detectors, activation and shielding optimization in ATLAS," CERN, Tech. Rep. ATL-GEN-2005-001, Jan 2005.
[6] The Tile Calorimeter Collaboration, "ATLAS Tile Calorimeter TDR," CERN, Tech. Rep. ATLAS-TDR-003, 1996.
[7] F. Ariztizabal et al., "Construction and performance of an iron-scintillator hadron calorimeter with longitudinal tile configuration," *Nuclear Instruments and Methods in Physics Research Section A*, vol. 349, pp. 384 – 397, 1994.
[8] R. Wigmans, *Calorimetry: energy measurement in particle physics*. Oxford: Clarendon Press, 2000.
[9] K. Anderson et al., "Design of the front-end analog electronics for the ATLAS tile calorimeter," *Nuclear Instruments and Methods in Physics Research A*, vol. 551, pp. 469–476, 2005.
[10] A. Cerqueira et al., "Analog system for building the first-level triggering signal provided by the hadronic calorimeter of ATLAS detector," *Nuclear Instruments and Methods in Physics Research Section A*, vol. 570, pp. 117–125, 2007.
[11] The ATLAS Muon Collaboration, "ATLAS muon spectrometer TDR," CERN, Tech. Rep. LHCC-97-22, 1997.
[12] R. Nicolaidou, B. Resende, "Muon track reconstruction in the ATLAS experiment," in *Conference Record for IEEE Nuclear Science Symposium*, vol. 1, Dresden, 2008, pp. 864–866.
[13] T. Ciodaro et al, "A receiver system for the TileCal muon signals," in *Conference Record for IEEE Nuclear Science Symposium*, vol. 1, Orlando, 2009, pp. 1–8.
[14] The ATLAS Collaboration, *Expected performance of the ATLAS experiment: detector, trigger and physics*. Geneva: CERN, 2009. [Online]. Available: http://arxiv.org/abs/0901.0512
[15] P. Adragna, et al, "Testbeam studies of production modules of the ATLAS Tile calorimeter," *Nuclear Instruments and Methods in Physics Research, A*, vol. 606, pp. 362–394, February 2009.
[16] J. Tront, *PSpice for basic circuit analysis*. McGraw-Hill, 2005, vol. 2.
[17] TileCal Collaboration, "ATLAS Experiment - Public Results. Approved Tile Calorimeter plots," https://twiki.cern.ch/twiki/bin/view/AtlasPublic/ApprovedPlotsTile.
[18] H. van Trees, *Detection, estimation, and modulation theory part I*. John Wiley & Sons, 2001.
[19] ——, *Detection, estimation, and modulation theory part III*. John Wiley & Sons, 2001.
[20] I. T. Jolliffe, *Principal component analysis*. Spring-Verlag, 2002.
[21] J. Lin, "Divergence measures based on the Shannon entropy," *IEEE Transactions on Information Theory*, vol. 37, pp. 145–151, 1991.
[22] T. Ciodaro et al, "A receiver system for detecting calorimeter signals under low signal-to-noise ratio conditions," in *Proceedings of the XXXIX International Congress and Exposition on Noise Control Engineering*, vol. 1, Lisbon, 2010, pp. 1–8.
[23] The ATLAS Collaboration, "Muon reconstruction performance," CERN, Geneva, Tech. Rep. ATLAS-CONF-2010-064, Jul 2010.